# Improved reliability from a plasma-assisted metal-insulator-metal capacitor comprising a high-*k* $HfO_2$ film on a flexible polyimide substrate†

**Jagan Singh Meena,[a] Min-Ching Chu,[a] Shiao-Wei Kuo,[b] Feng-Chih Chang[c] and Fu-Hsiang Ko*[a]**

*Received 26th August 2009, Accepted 18th December 2009*
*First published as an Advance Article on the web 26th January 2010*
**DOI: 10.1039/b917604g**

We have used a sol–gel spin-coating process to fabricate a new metal-insulator-metal (MIM) capacitor comprising a 10 nm–thick high-*k* thin dielectric $HfO_2$ film on a flexible polyimide (PI) substrate. The surface morphology of this $HfO_2$ film was investigated using atomic force microscopy and scanning electron microscopy, which confirmed that continuous and crack-free film growth had occurred on the film surface. After oxygen ($O_2$) plasma pretreatment and subsequent annealing at 250 °C, the film on the PI substrate exhibited a low leakage current density of $3.64 \times 10^{-9}$ A $cm^{-2}$ at 5 V and a maximum capacitance density of 10.35 fF $\mu m^{-2}$ at 1 MHz. The as-deposited sol–gel film was completely oxidized when employing $O_2$ plasma at a relatively low temperature (*ca.* 250 °C), thereby enhancing the electrical performance. We employed X-ray photoelectron spectroscopy (XPS) at both high and low resolution to examine the chemical composition of the film subjected to various treatment conditions. The shift of the XPS peaks towards higher binding energy, revealed that $O_2$ plasma treatment was the most effective process for the complete oxidation of hafnium atoms at low temperature. A study of the insulator properties indicated the excellent bendability of our MIM capacitor; the flexible PI substrate could be bent up to $10^5$ times and folded to near 360° without any deterioration in its electrical performance.

## 1. Introduction

Plastic circuits have received growing interest because they combine plastic substrates with new classes of organic materials using low-cost fabrication approaches, such as inkjet printing and liquid film casting.[1,2] They are considered to be a key emerging technology for this century with their potential as an ultralow-cost and light-weight alternative to Si wafers.[3,4]

In some instances, they are compatible with continuous, high-speed reel-to-reel fabrication, high mechanical flexibility, transparent to visible/UV radiation, and can allow the circuit board to conform to a desired shape or flex during its use.[5,6] Subsequently, plastic circuits appear to be the foundation for future electronic devices, such as electronic papers, wearable sensors, low-cost smart cards, radio frequency identification tags, and flexible arrays of plastic microphones.[7–9] Recently, in terms of their superior bending, it was found that flexible organic transistors can perform better than flexible inorganic transistors.[10,11] Reliability stress testing is a very important method for analyzing the bending and stretching properties of flexible devices designed for such applications as accurate sensors for hydrogen[12] or for integration into artificial muscles or biological tissues.[13]

The additional number of steps and high-temperature processing required to achieve high-performance flexible devices, however, has limited the rate of implementation of semiconductor devices fabricated on flexible organic substrates. In part, this problem can be solved by reducing the transistor size; for example, by reducing the thickness of the silicon dioxide ($SiO_2$) gate dielectric in proportion to the shrinkage of the gate length of 70 nm. Nevertheless, such a thin $SiO_2$-dielectric layer imposes severe constraints on the device performance because this thickness approaches the quantum-tunneling limit and decreases the reliability of the metal oxide semiconductor field effect transistors (MOSFETs).[14]

For a small system with scaled-down thickness, the need for advanced materials is progressively focusing on composite systems that maintain or enhance the device performance. To address the issue of the leakage current, hafnium oxide ($HfO_2$) has become one of the most promising candidates for use as an alternative gate dielectric to replace $SiO_2$. It exhibits high temperature stability and excellent insulator properties against heat and electricity. $HfO_2$ is attractive high-*k* dielectric material with relatively very high dielectric constant ($k \sim$ *ca.* 25) and wide band gap (*ca.* 5.68 eV) relative to that of $SiO_2$.[15,16] Among the various methods for preparing metal oxide film, dc sputtering,[17] atomic layer deposition (ALD),[18]

[a] *Institute of Nanotechnology, National Chiao Tung University, Hsinchu 300, Taiwan. E-mail: fhko@mail.nctu.edu.tw*
[b] *Department of Materials and Optoelectronic Science, National Sun Yat-Sen University, Kaohsiung 804, Taiwan*
[c] *Department of Chemistry, National Chiao Tung University, Hsinchu 300, Taiwan*

† Electronic supplementary information (ESI) available: Low resolution XPS spectra of sol-gel deposited $HfO_2$ film on Cr/PI substrate for as deposited-baking and annealing at 250 °C treated samples. See DOI: 10.1039/b917604g

 

physical vapor deposition (PVD),[19] and metal organic chemical vapor deposition (MOCVD)[20] appear to be the most useful new technologies. Sol–gel spin-coating is a very efficient approach toward smooth, crack-free films exhibiting excellent surface conformity and uniformity over large areas. In addition, such films can be fabricated at room temperature and normal pressure, obviating the need for high-vacuum systems.[21–23] The thin films are produced on a substrate by spin-coating or dip-coating; *i.e.*, a small puddle of the fluid resin is placed at the center of a substrate, which is then spun at high speed (typically *ca.* 3000 rpm). Dielectric films deposited at low temperature generally exhibit poorer properties and higher degrees of current leakage because of the many traps present within the film. Hence, high-temperature annealing (at *ca.* 600–800 °C) is traditionally required to improve the electrical properties of such thin films.[23] Plastic thin PI substrates, however, become damaged at the higher temperatures ($\geq$ 300 °C) employed during annealing or depositing the film because of their intrinsic low thermal compatibility. Thus, a challenge remains to develop a promising method to overcome these processing limitations. Several researchers have observed that oxygen ($O_2$) plasma treatment affects the performance of thin films deposited at low temperature through sol–gel spin-coating.[24,25] The electrical properties of such films can improve considerably after $O_2$ plasma exposure, with enhanced remnant polarization and decreased leakage current density.

In this study, we developed a low-temperature $O_2$ plasma–enhanced method for preparing a $HfO_2$ thin film–based MIM capacitor fabricated on a flexible organic PI substrate using sol–gel spin processing. To determine the insulator properties of the film, we determined their current density–electric field (*J–E*) and capacitance–voltage (*C–V*) characteristics. We also investigated the $O_2$ plasma oxidation growth mechanism in different kinetic regimes to understand the surface oxidation process. Moreover, X-ray photoelectron spectroscopy (XPS) suggested the feasibility of using this low-temperature processing approach toward achieving high-performance flexible devices. A test revealed that the capacitor on the PI surface performed reliably after bending up to $10^5$ times.

## 2. Experimental

### 2.1 Materials and fabrication

Plastic 30 μm–thick DuPont Kapton® PI films were used as flexible substrates. They were cleaned ultrasonically with ethanol (Fluka; water content: <0.1%) for 30 min and deionized water for 10 min and then high-pressure $N_2$ gas was used to remove the water and any remaining particles from the PI surface. Next, Cr (thickness: 10 nm; adhesion layer) and Au (thickness: 100 nm) were deposited for the gate electrode over the PI substrate using a thermal coater. To deposit the high-*k* $HfO_2$ film, a sol–gel solution was prepared by dissolving $HfCl_4$ (98%, Aldrich, USA) in ethanol (95%) at a suitable concentration. We added ethanol (10 mL) as the solvent to yield a molar ratio of $HfCl_4$ to $C_2H_5OH$ of 1 : 1000; after adding a magnetic stirrer, the solution was heated under reflux while stirring for 30 min. The film was grown by spin-coating the sol–gel solution over PI at 3000 rpm for 30 s at room temperature using a Clean Track Model-MK8 (TEL, Japan) spin coater. The as-prepared samples were treated with $O_2$ plasma for 2 min in an oxygen plasma reactor (Harrick Scientific Corp.), which supplied a plasma power of 30 W; subsequent annealing was performed in the presence of $O_2$ at 250 °C for 12 h (refer, OPT/A). Finally, 300 nm–thick Al films were patterned as the top electrodes using a shadow mask and a thermal coater.

### 2.2 Characterization

The surface morphology of the high-*k* $HfO_2$ film over PI was evaluated using scanning electron microscopy (FE-SEM, JOEL JSM-5410, operated at 5 kV) and atomic force microscopy (AFM, Digital Instruments Nanoscope, D-5000) at a scan size of 2 μm and a scan rate of 1 Hz. We used ellipsometry techniques to measure the thickness of the $HfO_2$ film. We used XPS to analyze the chemical bonding of the elements of interest under various treatment conditions. To characterize the leakage currents and capacitances of the films, we prepared them in the metal-insulator-metal (MIM) configuration represented in Fig. 1(a). The *J–E* measurements were performed using an Agilent-4156 probe station; the capacitance was measured using an HP-4284A *C–V* analyzer. Fig. 1(b) displays a photograph of the flexible capacitor device on a 30 μm–thick PI substrate under a large surface strain, but without any cracks appearing on the surface; the inset reveals the bending characteristics of this capacitor with unlimited fold-up to an angle of 360°. Thus, it is possible to apply a large mechanical strain to the devices fabricated onto the plastic substrate to evaluate their test strain. A customized bending machine (depicted and described in detail elsewhere in this text) was used to perform bending tests with the flexible MIM capacitor device.

## 3. Results and discussion

### 3.1 Film quality and roughness

The $HfO_2$ film was prepared by spin-coating a sol–gel mother solution onto the chromium (Cr) coated flexible PI substrate used as a gate insulator layer. Cr was used to make firm adhesion between PI and sol–gel derived $HfO_2$ film.[26] Fig. 2(a) and (b) present top-view SEM images of the as-deposited, sol–gel spin-coated films after baking at 80 °C and annealing at 250 °C for 12 h. Many trap states are present over both film surfaces, suggesting that they would directly affect the

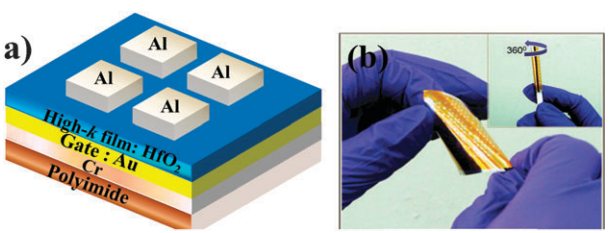


**Fig. 1** (a) Schematic representation of an MIM capacitor featuring a high-*k* $HfO_2$ thin film on a PI substrate; (b) photograph of our MIM capacitor on the flexible ultra-thin PI substrate; inset: unlimited bend test up to an angle of 360°.

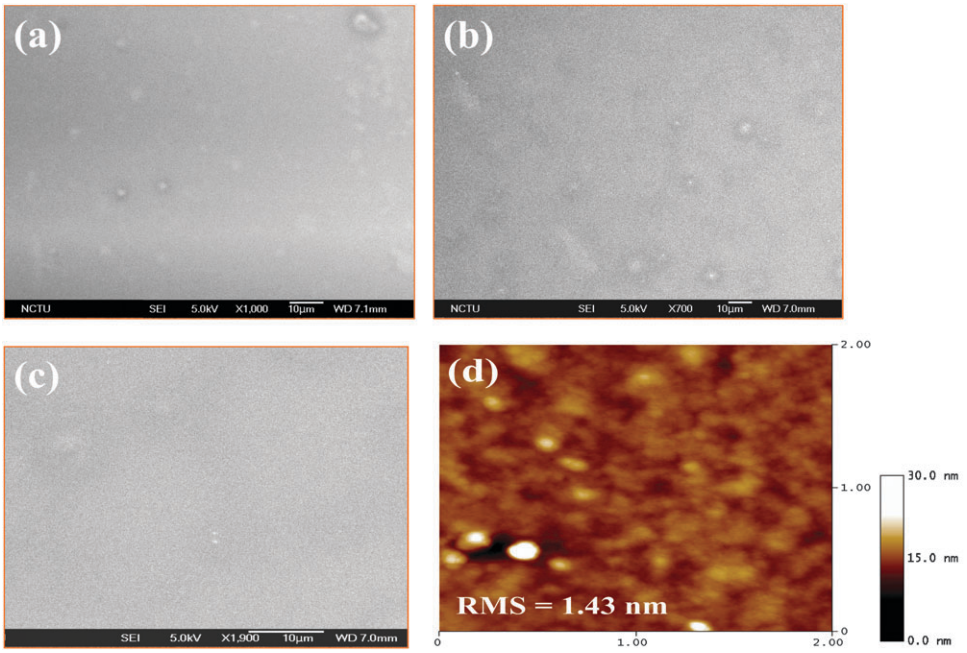


**Fig. 2** (a–c) Top-view SEM images of as-deposited $HfO_2$ films on Cr/PI substrates after (a) baking, (b) annealing at 250 °C for 12 h, (c) sequential $O_2$ plasma treatment and annealing at 250 °C for 12 h (OPT/A), (d) tapping-mode AFM image of the film subject to OPT/A-treatment.

electrical performance of the device. When $O_2$ plasma pretreatment was employed for 2 min on the as-grown sol–gel film and then annealing was performed at 250 °C for 12 h (abbreviated as OPT/A), a clean surface was generated. Fig. 2(c) displays the well-ordered, smooth, and crack-free $HfO_2$ film that was grown successfully on the PI substrate. The surface roughness of the insulator layer is another important factor affecting the performance of MOS devices. Here, we used tapping-mode AFM on a length scale of 2 × 2 μm to determine the surface roughness of the film. Fig. 2(d) indicates that the surface roughness of the film surface of the sample treated with OPT/A was 1.43 nm. The thickness of $HfO_2$ film subjected to OPT/A-treatment was measured to be 10 nm using ellipsometry techniques.

### 3.2 Effect of $O_2$ plasma on $HfO_2$ thin film formation

We measured the quantitative leakage current and capacitance to evaluate the dielectric performance of the high-$k$ $HfO_2$ film in the MIM configuration. Fig. 3(a) displays the $J$–$E$ characteristics for flexible MIM capacitors prepared under various sample treatment conditions. The as-deposited samples that were baked at 80 °C and annealed in the presence of $O_2$ at 250 °C for 12 h did not have sufficiently high thermal budgets and, thus, their breakdown electric fields were relatively low and their leakage current densities were very high ($1.69 \times 10^{-5}$ and $1.59 \times 10^{-7}$ A cm$^{-2}$, respectively, at an applied voltage of 5 V). The leakage current density was $3.64 \times 10^{-9}$ A cm$^{-2}$ for the sol–gel-deposited $HfO_2$ film subjected to OPT/A treatment conditions. The baking-only treated $HfO_2$ film exhibited the largest leakage current among these treated films because it had poor dielectric characteristics and numerous traps present within the film. A slight improvement in the electrical characteristics occurred for the annealing-only treated sample. The leakage current density decreased when the sample was treated with $O_2$ plasma for 2 min and then annealed at 250 °C for 12 h, indicating that the poorer leakage properties of the other two treated samples arose because of the existence of numerous traps over their film surfaces. The breakdown electric field (*ca.* 2.3 MV cm$^{-1}$) also increased when the sample was subjected to the OPT/A treatment conditions. The OPT/A-treated sample exhibited excellent electrical characteristics on the PI substrate because (i) the wet hafnium film underwent a high degree of oxidation under $O_2$ plasma treatment and (ii) subsequent annealing led to a reduction in the number of traps. The low leakage current of our flexible MIM capacitor is comparable with that of silicon- and glass-based capacitor devices.[27–29]

To understand the carrier transport mechanisms of the OPT/A-treated hafnium dielectric film, Fig. 3(b) presents a plot of ln($J$) with respect to the square root of the applied electric field ($E^{1/2}$). For standard Schottky–Richardson (SR) emission, the plot of ln($J$) *versus* $E^{1/2}$ should be linear; can be expressed as[30]

$$J = A * T^2 \exp\left[\frac{-q(\phi_B - \sqrt{qE/4\pi\varepsilon_r\varepsilon_0})}{KT}\right] \quad (1)$$

where $A$ is the effective Richardson constant, $q\phi_B$ is the Schottky barrier height, $\varepsilon_0$ is the permittivity in a vacuum, and $\varepsilon_r$ is the dynamic dielectric constant of $HfO_2$. SR emission induced by the thermionic effect is caused by electron transport across the potential energy barrier, as indicated in the inset to Fig. 3(b); it is independent of traps and dominates the conduction mechanism.[31]

The conversion of the current transport mechanism from trap-assisted tunneling for the as-deposited and annealing-only samples to SR emission for the OPT/A sample demonstrates theoretically that the sol–gel hafnium film was

 

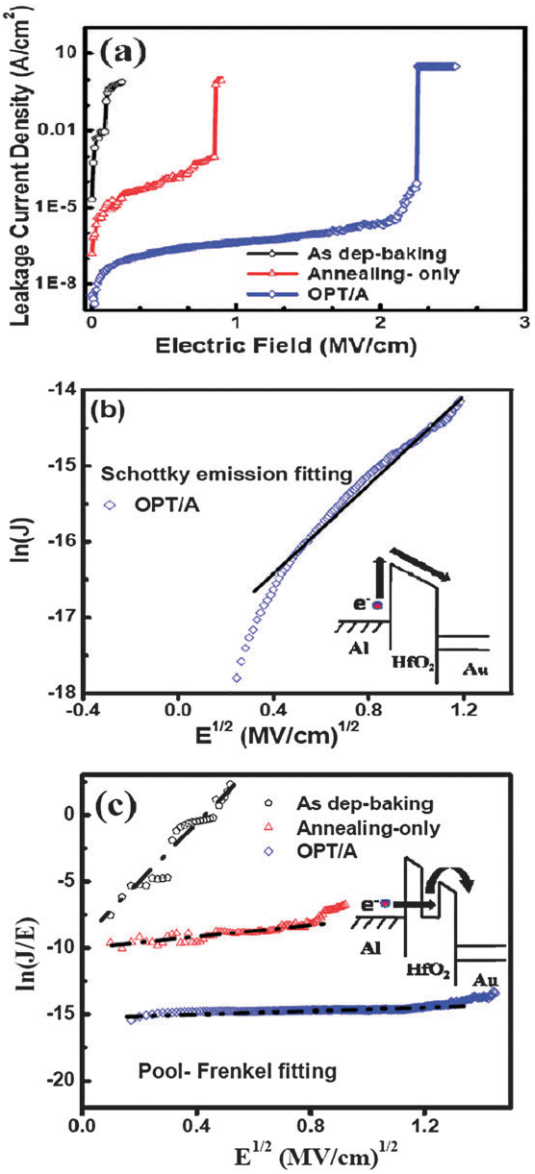


**Fig. 3** (a) Plots of leakage current density *versus* electric field under an applied positive voltage for samples prepared using all three treatment conditions. (b) Plot of ln($J$) *versus* the square root of the electric field ($E^{1/2}$) for the OPT/A-treated sample. (c) Plot of ln($J/E$) *versus* ($E^{1/2}$) for the three samples. The corresponding schematic energy band diagram is presented to explain the S–R and P–F emissions.

oxidized and traps were completely terminated. Fig. 3(c) presents plots of ln($J/E$) *versus* $E^{1/2}$ for the baking, annealing, and OPT/A-treated $HfO_2$ films; the inset displays a schematic energy band diagram that elucidates the leakage transport mechanisms. It is believed that the Poole–Frenkel (PF) emission is due to field-enhanced thermal excitation of trapped electrons in the bulk of the insulator. The conduction process at higher voltages is likely due to the PF emission,[32] which is described by the equation

$$J = CE\exp\left(\frac{-q\phi_t}{kT}\right)\exp\left[\frac{1}{rkT}\sqrt{\frac{q^3}{\pi\varepsilon_0 K_T}}\sqrt{E}\right] \qquad (2)$$

where $C$ is a constant, $q$, $k$, $T$, and $E$ represent the electronic charge, the Boltzmann constant, the temperature, and the electric field, respectively, $\varepsilon_0$ denotes the permittivity of free space, $K_T$ is the high-frequency dielectric constant (square of the refractive index), and $\phi_t$ is the energy barrier separating the traps from the conduction band. The coefficient $r$ is introduced in the expression to take into account the influence of the trapping or acceptor centers ($1 \leq r \leq 2$). As a result, the plot of ln($J/E$) as a function of $E^{1/2}$ in Fig. 3(c) reveals that the as-deposited baking- and annealing-only samples possessed huge numbers of traps, which decreased the band gap in the $HfO_2$ films because the thermal budget was insufficient to form dense and trap-free dielectric layers. For the as-deposited sample, the linear dependence began at a very low electric field (*ca.* 0.2 MV cm$^{-1}$). The traps within the $HfO_2$ film were not reduced after baking-only treatment; the device featured a high leakage current and a low breakdown electric field. For annealing-only sample, the traps inside the $HfO_2$ films had been reduced and the current transport mechanism was improved from trap-assisted tunneling to FP emission, but this improvement remained less obvious and resulted in poorer dielectric properties. Under treatment with $O_2$ plasma, the PF emission was gradually restrained. Finally, the current transport mechanism was replaced by SR emission after OPT/A treatments of the as-grown film. These findings confirm that the number of traps was minimized within the low temperature-deposited $HfO_2$ film after plasma treatment.

Fig. 4 displays the $C$–$V$ characteristics of our flexible MIM capacitor. Here, we have only measured the capacitance density for the OPT/A-treated $HfO_2$ film; the maximum measured capacitance density was 10.35 fF μm$^{-2}$ at 1 MHz. The high capacitance of this low temperature-deposited $HfO_2$ film after OPT/A treatment would allow its future flexible electronic devices to be operated in the low voltage regime. In addition, according to the capacitance and thickness data, we estimated the dielectric constant ($k$) of the $HfO_2$ film to be 11.7. The observation of the calculated value of $k$ is lower than that of pure $HfO_2$ film, but consistent with the previous results for calculated dielectric constant of sol–gel derived $HfO_2$ films.[33–35] The calculated value of $k$ is sharply decreased as the film thickness is very low ($\sim$10 nm) by means of Lorenz's local field theory.[34] However, the $k$ value for our sol–gel derived flexible capacitor is still higher than that of $SiO_2$ on silicon wafer ($k$ = 3.8). Thus, one approach is the use of materials with dielectric constants higher than that of $SiO_2$ materials as thin-film dielectric materials, whereby the $HfO_2$ dielectric materials with dielectric constants of about 11.7 or above, demonstrate the possibility to replace the conventional $SiO_2$-based materials.

We used a plasma oxidation growth mechanism at low temperature to examine the influence of $O_2$ plasma on the as-deposited hafnium film. It was expected that there would be a direct interaction of active atoms and molecules in the plasma ($O^+$, $O^-$, O, $O_2$, free electrons, *etc.*) with organic species in the sample.[36] The sol–gel solution comprising $HfCl_4$ dissolved into alcohol and was coated over the flexible PI substrate. Fig. 5 displays the possible chemical transformation, the hydrolysis and condensation reactions with an exothermic elimination of HCl; which also includes

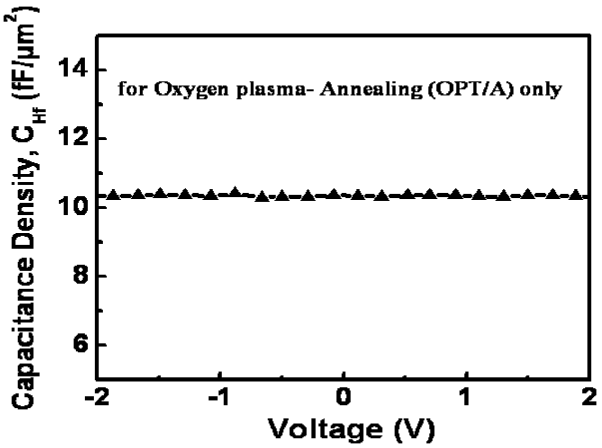


**Fig. 4** Plot of capacitance density (*C*) as a function of the applied voltage (*V*) for the OPT/A-treated capacitor device.

decomposition reactions for $O_2$ plasma on the as-deposited sol–gel film. In (I) step, the as-deposited film existed in the solid-state, presumably with a HO–Hf–O–Hf–OR model based structure. It appeared that a homogeneous network of –O–Hf–O–Hf–O– bonds had not developed in the thin film. In steps (ii) and (iii), the power plasma induced the formation of some active oxygen species that reacted with model structure of HO–Hf–O–Hf–OR, resulting in partial oxidation to hafnium oxide. The imposing plasma gradually oxidized the as deposited thin film. In the final step (iv), the film surface was near-complete oxidation to $–(O–Hf–O)_n–$ using plasma oxidation; the organic parts were mostly removed. Oxidation through $O_2$ plasma treatment of the thin film occurred at lower temperature than conventional high-temperature annealing on thin film; this process allows high-performance electronic devices to be fabricated on plastic substrates.

To obtain a better understanding of the $O_2$ plasma effect, we used XPS analysis to examine the chemical composition of the films obtained under different treatment conditions. Fig. 6 displays high-resolution spectra of the Hf 4f energy levels of the three samples. The spectra were deconvoluted into two spin–orbit doublet peaks for the Hf $4f^{7/2}$ and Hf $4f^{5/2}$ energy levels at different binding energies of the Hf–O bonds. For the baking-only treatment (Fig. 6a), the peaks for the $4f^{7/2}$ and $4f^{5/2}$ binding energies were detected at 16.1 and 17.6 eV, respectively. After annealing-only treatment (Fig. 6b), these binding energies were raised to 16.4 and 17.9 eV, respectively. Furthermore, excellent advancement of the O–Hf–O bonds was achieved through $O_2$ plasma treatment (Fig. 6c), the binding energies of $4f^{7/2}$ and $4f^{5/2}$ were raised to 16.8 and 18.5 eV, respectively; fit well more likely to previous studies.[37,38] Compared to the as deposited sample, the Hf 4f spectrum of the plasma treated $HfO_2$ film is shifted roughly 0.7 eV to the higher binding energy (BE). The shift toward higher BE for the Hf–O bonds suggests that oxygen plasma treatment introduced some bonding structures [*i.e.*, $–(O–Hf–O)_n–$ units] for the complete oxidation of the Hf atoms.[39] Fig. 6(b) and (c) imply that $O_2$ molecules reacted with the Hf dangling bonds (or traps) to form stronger Hf–O bonds and that subsequent annealing in the $O_2$ plasma effectively transported $O_2$ molecules into the $HfO_2$ film to passivate the traps. In addition, we recorded the low-resolution XPS spectra for the Hf 4f bonds for $HfO_2$ film subjected to as-prepared, annealing and OPT/A-treatment conditions to examine its chemical composition. Fig. S1† displays the spectrum of the as-deposited film with a broad O(1s) peak at around 531 eV and the O(1s) peak for an

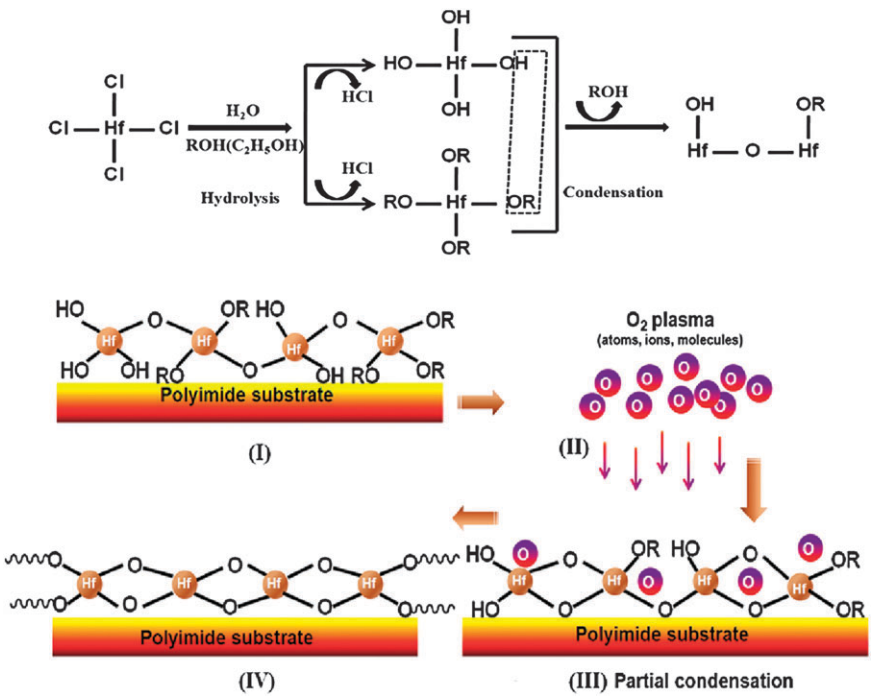


**Fig. 5** Schematic representation of the $O_2$ plasma growth mechanism for sol–gel-derived spin-coated $HfO_2$ film.

 

annealed-only sample at around 532.3 eV. In the as-deposited film, the intense C(1s) peak at around 286.6 eV is attributed to C–O–H from the ethanol solvent. This observation is in excellent agreement with the reported literature value.[40] The C(1s) peak for annealed sample is at around 285.0 eV and band intensity significantly decreases than the as deposited film due to solvent evaporation. Fig. 7 reveals that the sample consisted of hafnium, oxygen, and a small amount of contaminating carbon; no other impurities (*e.g.*, chloride ions) were present on the film surface. This good composition is similar to those reported previously.[14,41] We calibrated the binding energies by setting the residual C(1s) peaks at 284.6 and 288.0 eV, and the O(1s) peak at 533.9 eV. We find the band intensity of O(1s) peak remains strong and C(1s) peak decreases upon plasma treatment. The existence of low intense C(1s) peak can be attributed to a partially oxidized carbon species with a slight peak broadening, since the oxygen atoms bond to a portion of carbon. The peak appearing at the higher BE of 288.0 eV is due to C–O related bonding as shown in the inset of Fig. 7. Although the C(1s) peak at 284.6 eV may be associated with (C–H) bond (Inset: Fig. 7), and it remains unchanged even after plasma treatment. This indicates the availability of residual carbon species is still found over the film. This spectroscopic result reveals that the content of defects was much reduced after subjecting the sample to OPT/A treatment and subsequent annealing to form the complete composite oxide hafnium film (*i.e.*, $HfO_2$). The XPS analysis confirms the chemical reaction of the $HfO_2$ film prepared through the $O_2$ plasma-induced transformation of the sol–gel-derived thin film. This approach possesses one particular advantage over other standard plasma oxidized technologies: it provides a higher rate of oxidation of the wet-state of the film at lower treating temperatures.

### 3.3 Bending treatment for mechanical flexibility and stability

Fig. 8 displays the leakage current densities for the OPT/A-treated $HfO_2$ films subjected to four different bending times. We measured the leakage currents prior to bending treatment to understand the performance of the initial MIM capacitor, revealing that the $HfO_2$ film exhibited superior electrical performance. The film retained its low leakage current density (*ca.* $10^{-9}$ A cm$^{-2}$) after bending the device $10^3$ or $10^5$ times. All of the curves overlapped, with no further increments in the leakage current density for either positive or negative biasing conditions after bending the capacitor up to $10^5$ times. Indeed, the $HfO_2$ film over PI exhibited superior reliability after bending the device. The photograph in the inset to Fig. 8 displays our homemade bending machine and our flexible capacitor under an applied strain; the counter of the number of bends and the set time are also indicated. After performing the bending test, the breakdown field ($E$) remained the same as was prior to bending (*ca.* 2.25 MV cm$^{-1}$), indicating that using the spin-coating process to form the $HfO_2$ films provides superior electrical characteristics and reliability for the MIM structure. Again, we conclude from this result that the performance of our flexible-base capacitor device is comparable to that of silicon and glass-based capacitor devices, even after folding or bending the sample unlimitedly. To the best of our knowledge, there are no parallel reports describing reliability tests of flexible capacitors employing $HfO_2$ films as insulator layers that exhibit satisfactory electrical properties.

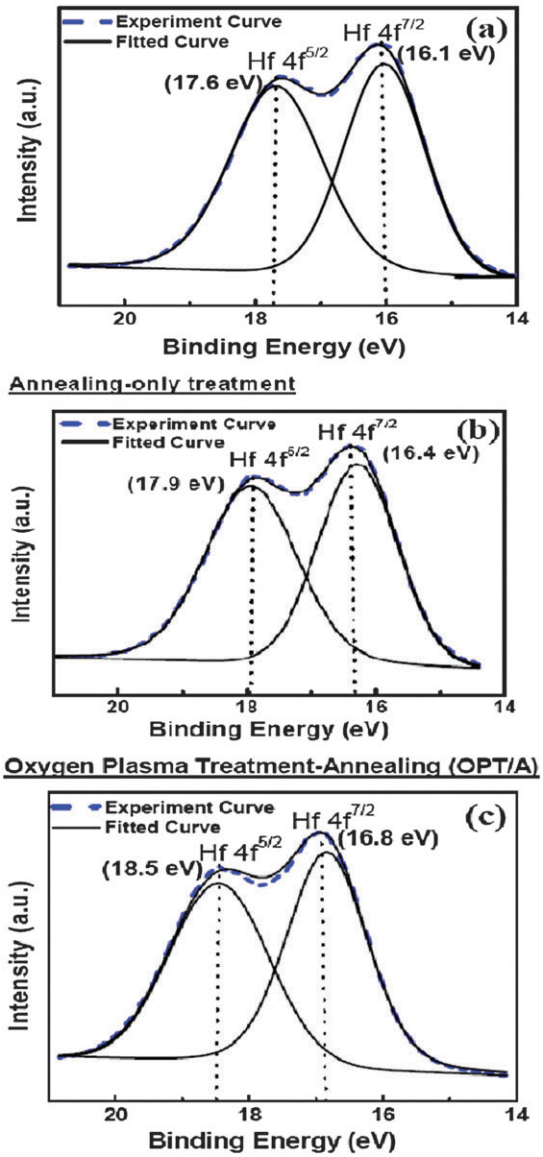


**Fig. 6** High-resolution XPS spectra of the Hf 4f energy levels for as-deposited $HfO_2$ films subjected to (a) baking, (b) annealing at 250 °C for 12 h, and (c) OPT/A-treatment. The dotted curve represent the experimental data; solid curves represent the fitted peaks and the summarized results of the fitted data.

### 3.4 Electrical performance of the flexible capacitor under convex-and concave-type bending conditions

We tested two additional features of our sol–gel-derived capacitor on a flexible substrate to explore its feasibility for use in practical applications. Namely, we measured the current density in both convex (Fig. 9a) and concave (Fig. 9b) settings, varying the radii of curvature (RC) from 1 to 3.5 cm. During

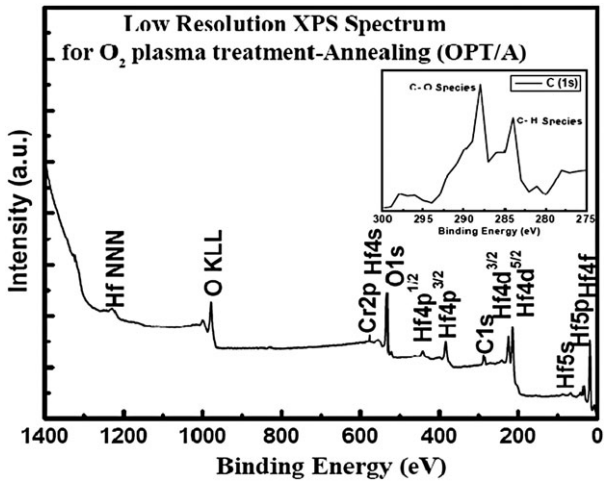


**Fig. 7** Low resolution XPS spectrum of the OPT/A-treated $HfO_2$ film on the PI substrate. Inset: XPS spectra in the BE regions of C (1s).

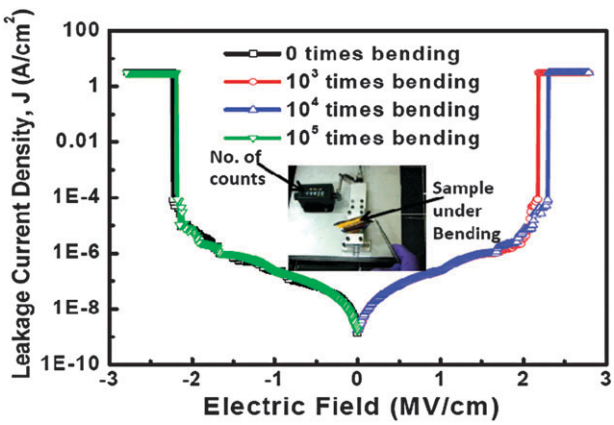


**Fig. 8** Leakage current density plotted as a function of the electric field, measured at both negative and positive biased voltages, for the OPT/A-treated flexible MIM capacitor after being subjected to repeated bendings for various times.

the manufacturing process, a foil was used as a substrate support to provide these specific bending conditions. We observed the electrical characteristics, such as the leakage current density ($<10^{-8}$ A $cm^{-2}$) and breakdown field (*ca.* 2.25 MV $cm^{-1}$) under both negative and positive biasing conditions. The sol–gel-derived $HfO_2$ film obtained after OPT/A treatment behaved as a stable electrical insulator, even after bending the device at the different radii of curvature. Under the RC (3.5 cm) concave conditions, the change in the thickness of the film, relative to that of the flat device, was *ca.* 0.00001%. Thus, we conclude that the thickness of the $HfO_2$ film remained unchanged when the device was subjected to 3.5 cm concave- or convex-type bending conditions. Even when the sample was bent under RC (1 cm) concave conditions, the variation in the $HfO_2$ film thickness was only *ca.* 0.0001%. Bending led to nearly no changes in the electrical characteristics under the various RC concave or convex conditions. The low deviations in leakage current density ($<10^{-8}$ A $cm^{-2}$) upon bending between 1 and 3.5 cm reveal

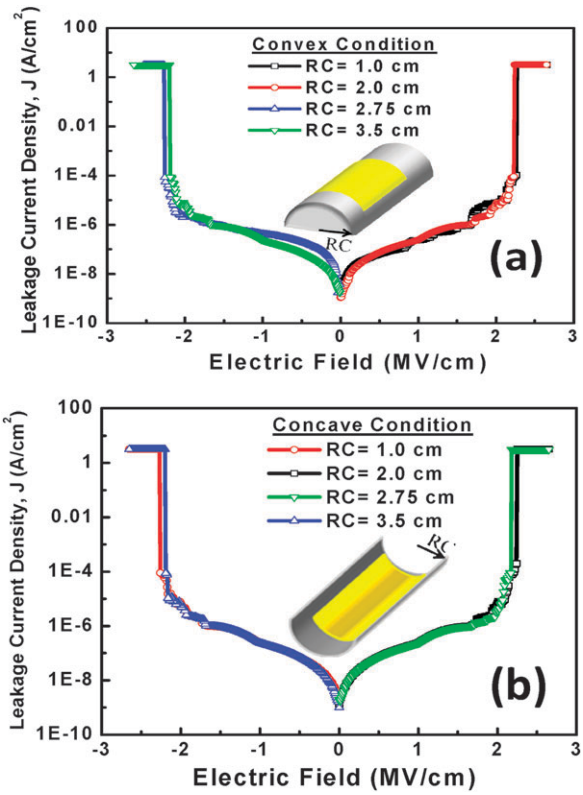


**Fig. 9** Leakage current density measurements for (a) convex and (b) concave devices; radii of curvature (RC) were varied from 1 to 3.5 cm.

that no clear trend can be attributed to repeated driving under either set of conditions.

## 4. Conclusions

We have prepared MIM-structured capacitors using ultrathin 10-nm high-*k* $HfO_2$ films deposited through sol–gel spin-coating on flexible PI substrates. The material properties and electrical performances of these films verified the effectiveness of applying low temperature plasma processing to the fabrication of future soft devices. The $HfO_2$ film exhibited a low leakage current density of $3.64 \times 10^{-9}$ A $cm^{-2}$ at 5 V and a maximum capacitance density of 10.35 fF $\mu m^{-2}$ at 1 MHz. The electrical behavior analyzed under various bending treatment conditions revealed that our flexible capacitor functioned independent of the bending conditions (*i.e.*, the number of bends and the bending radii). The electrical characteristics of our flexible MIM capacitors suggest they are comparable with those of silicon- and glass-based capacitor devices, even after bending the devices up to $10^5$ times. We believe that amorphous high-*k* $HfO_2$ is a leading candidate for use in future flexible devices as a stable gate dielectric fabricated through processing at low temperatures.

## Acknowledgements

This investigation was generously supported by funds provided by the National Science Council of Taiwan (97-2120-M-009-003 and 97-2218-E-009-002).

 

## References


1 Y. Chen, J. Au, P. Kazlas, A. Ritenour, H. Gates and M. McCreary, *Nature*, 2003, **423**, 136.
2 S. H Ko, H. Pan, C. P Grigoropoulos, C. K Luscombe, J. M J Frechet and D. Poulikakos, *Nanotechnology*, 2007, **18**, 345202.
3 J. Jang, K. Cho, S. H. Lee and S. Kim, *Nanotechnology*, 2008, **19**, 015204.
4 H. Lim, W.-J. Cho, C.-S. Ha, S. Ando, Y.-K. Kim, C.-H. Park and K. Lee, *Adv. Mater*., 2002, **14**, 1275.
5 A. Fian, A. Haase, B. Stadlober, G. Jakopic, N. B. Matsko, W. Grogger and G. Leising, *Anal. Bioanal. Chem*., 2008, **390**, 1455.
6 S.-M. Lee, G. Grass, G.-M. Kim, C. Dresbach, L. Zhang, U. Gosele and M. Knez, *Phys. Chem. Chem. Phys*., 2009, **11**, 3608.
7 J. A. Rogers, *Science*, 2001, **291**, 1502.
8 D. J. Lichtenwalner, A. E. Hydrick and A. I. Kingon, *Sens. Actuators, A*, 2007, **135**, 593.
9 V. Privitera, S. Scalese, A. La Magna, A. Pecora, M. Cuscunà, L. Maiolo, A. Minotti, D. Simeone, L. Mariucci, G. Fortunato, L. Caristia, F. Mangano, S. Di Marco, M. Camalleri, S. Ravesi, S. Coffa, M. G. Grimaldi, R. De Bastiani, P. Badalà and S. Bagiante, *J. Electrochem. Soc*., 2008, **155**, H764.
10 T. Sekitani, Y. Kato, S. Iba, H. Shinaoka, T. Someya, T. Sakurai and S. Takagi, *Appl. Phys. Lett*., 2005, **86**, 073511.
11 Y. Watanabe, H. Iechi and K. Kudo, *Appl. Phys. Lett*., 2006, **89**, 233509.
12 Y. Sun and H. H. Wang, *Adv. Mater*., 2007, **19**, 2818.
13 Argonne National Laboratory (US), *Department of Energy Laboratory*, *ARGONNE*, *Ill*, Chicago, Argonne, LLC, 2007, April 2.
14 A. R. Phani, M. Passacantando and S. Santucci, *J. Non-Cryst. Solids*, 2007, **353**, 663.
15 Z. J. Wang, T. Kumagai, H. Kokawa, M. Ichiki and R. Maeda, *J. Electroceram*., 2007, s 10832-007-9228.
16 A. Dkhissi, G. Mazaleyrat, A. Este've and M. D. Rouhani, *Phys. Chem. Chem. Phys*., 2009, **11**, 3701.
17 C.-T. Tsai, T.-C. Chang, K.-T. Kin, P.-T. Liu, P.-Y. Yang, C.-F. Weng and F.-S. Huang, *Appl. Phys. Lett*., 2008, **103**, 074108.
18 S. Kim, J. Kim, J. Choi, H. Kang and H. Jeon, *J. Vac. Sci. Technol*., 2006, **B24**(3), 1071.
19 H. Watanable, S. Horie, T. Minami, N. Kitano, M. Kosuda, T. Shimura and K. Yasutake, *Jpn. J. Appl. Phys*., 2007, **46**(4b), 1910.
20 D. H. Triyoso, M. Ramon, R. I. Hegde, D. Roan, R. Garcia, J. Baker, X.-D. Wang, P. Fejes, B. E. White, Jr. and P. J. Tobin, *J. Electrochem. Soc*., 2005, **152**, G203.
21 S.-M. Chang and R.-a. Doong, *Thin Solid Films*, 2005, **17**, 489.
22 H.-C. You, T.-H. Hsu, F.-H. Ko, J.-W. Huang, W.-L. Yang and T.-F. Lei, *IEEE Electron Device Lett*., 2006, **27**, 799.
23 K. Suzuki and K. Kato, *J. Am. Ceram. Soc*., 2009, **92**, S162.
24 K.-K. Han, S. W. Lee and H. H. Lee, *Appl. Phys. Lett*., 2006, **88**, 233509.
25 C. Zhang, P. Chen, B. Sun, W. Li, B. Wang and J. Wang, *Appl. Surf. Sci*., 2008, **254**, 5776.
26 S. H. Kim, S. H. Cho, N.-E. Lee, H. M. Kim, Y. W. Nam and Y.-H. Kim, *Surf. Coat. Technol*., 2005, **193**, 101.
27 X. Yu, C. Zhu, H. Hu, A. Chin, M. F. Li, B. J. Cho, D.-L. Kwong, P. D. Foo and M. B. Yu, *IEEE Electron Device Lett*., 2003, **24**, 63.
28 Y. Aoki and T. Kunitake, *Adv. Mater*., 2004, **16**, 118.
29 N. Kameda, T. Nishiguchi, Y. Morikawa, M. Kekura, H. Nonaka and S. Ichimura, *J. Electrochem. Soc*., 2007, **154**, H769.
30 S. M. Sze, *Physics of Semiconductor Devices*, Wiley, New York, 2nd edn, 1981.
31 P. R. Emtage and W. Tantraporn, *Phys. Rev. Lett*., 1962, **8**, 267.
32 C. Chaneliere and J. L. Autran, *J. Appl. Phys*., 1999, **86**, 480.
33 K. J. Wang and K. Y. Cheong, *Appl. Surf. Sci*., 2008, **254**, 1981.
34 Y. Aoki, T. Kunitake and A. Nakao, *Chem. Mater*., 2005, **17**, 450.
35 J. Tardy, M. Erouel, A. L. Deman, A. Gagnaire, V. Teodorescu, M. G. Blanchin, B. Canut, A. Barau and M. Zaharescu, *Microelectron. Reliab*., 2007, **47**, 372.
36 J. Huang, I. Ichinose, T. Kunitake and A. Nakao, *Langmuir*, 2002, **18**, 9048.
37 Y. W. Kim, Y. Roh, J.-B. Yoo and H. Kim, *Thin Solid Films*, 2007, **515**, 2984.
38 O. Renault, L. Fourdrinier, E. Martinez, L. Clavelier, C. Leroyer, N. Barrett and C. Crotti, *Appl. Phys. Lett*., 2007, **90**, 052112.
39 J. F. Moulder, W. F. Stickle, P. E. Sobol and K. D. Bomben, *Handbook of X-Ray Photoelectron Spectroscopy*, Physical Electronics, Inc., 1995.
40 J. C. Vickerman, *Surface Analysis—The Principal Techniques*, John Wiley & Sons, Inc., 2003, pp. 51–70.
41 T. Brezesinski, B. Smarsly, K. Iimura, D. Grosso, C. Boisser, H. Amenitsch, M. Antonietti and C. Sanchez, *Small*, 2005, **1**, 889.